Sensors and Actuators A 153 (2009) 24–32

Contents lists available at ScienceDirect

Sensors and Actuators A: Physical

journal homepage: www.elsevier.com/locate/sna

Microphone based on Polyvinylidene Fluoride (PVDF) micro-pillars and patterned electrodes

J. Xu [a], M.J. Dapino [a,*], D. Gallego-Perez [b], D. Hansford [b]

[a] Department of Mechanical Engineering, The Ohio State University, Columbus, OH 43210, USA
[b] Department of Biomedical Engineering, The Ohio State University, Columbus, OH 43210, USA

ARTICLE INFO

Article history:
Received 30 December 2008
Received in revised form 11 April 2009
Accepted 11 April 2009
Available online 24 April 2009

Keywords:
PVDF
Microphone
Sensor array
Nano-indentation

ABSTRACT

This article is focused on the development of an acoustic pressure sensor with extremely high sensitivity and small footprint. We propose a sensor design consisting of micron-sized Polyvinylidene Fluoride (PVDF) pillars which generate a charge when subjected to normal stresses associated with acoustic waves. A rigid membrane placed between the micro-pillars and the acoustic medium ensures high mechanical coupling. The electrode covering the micro-pillars is patterned to decrease the capacitance, and hence increase the sensitivity of the sensor. The key sensor parameters (diameter and height of the micro-pillars, gap between pillar edges, and number of pillars) are determined through a constrained optimization algorithm in which the penalty function is the sensor footprint. The algorithm incorporates the effects of mechanical and electrical properties of the sensor and conditioning amplifier. Details of the fabrication process are described. Nano-indentation tests demonstrate that the PVDF micro-pillar sensor exhibits piezoelectric responses under an applied voltage or strain, thus demonstrating the sensor concept.
© 2009 Elsevier B.V. All rights reserved.

1. Introduction

Existing commercial microphones are capable of either high sensitivity or broad frequency bandwidth. Typical specifications for the former category include a sensitivity of about 50 mV/Pa and a frequency range of 10 kHz, whereas transducers in the latter category exhibit a sensitivity of about 1 mV/Pa and a frequency range of 70 kHz. It is emphasized that the above sensitivities include the gain provided by the built-in amplifier placed inside of the microphone case. These microphones tend to be large, with typical geometries having a diameter of 12 mm. While these devices work well in many applications, there is a need for acoustic sensors capable of exhibiting high sensitivity and broad frequency bandwidth, while simultaneously having a much smaller size than the existing designs.

Such microphones would enable new techniques for the measurement of noise-source characteristics, for example by means of extremely dense microphone arrays capable of measuring with great accuracy both pressure amplitude and direction. Such techniques will be crucial for guiding and validating the development of accurate noise prediction tools and effective suppression techniques [1,2].

One realization of microphones is electronic stethoscopes, which are commonly used for clinical auscultation and real-time monitoring of the human respiratory system. A significant volume of research has been devoted to the analysis of lung sounds based on empirical information of normal and abnormal lung sounds [3,4]. Electronic stethoscope arrays for measurement of breathing sounds are of great interest due to their non-invasive nature, yet the utilization of these arrays for real-time monitoring of lung sounds is confined to large sounds fields in adults. The existing electronic stethoscopes are too bulky, typically 25 mm in diameter, for utilization in infants and small children.

Cochlea-inspired transducers investigated by Grosh et al. [5,6] could achieve levels of miniaturization not possible with existing devices. A flexible tensioned membrane with an exponentially tapered width is employed to obtain a varying acoustic impedance, which can achieve cochlear-like frequency-position mapping. A rigid-walled duct filled with silicone oil is implemented to mimic the environment of the passive mammalian cochlea. Arnold et al. [1] designed a piezoresistive silicon microphone for aeroacoustic measurements that has small size, high dynamic range, large frequency bandwidth, and low power consumption. The microphone consists of four dielectrically isolated, single crystal silicon piezoresistors mounted on the top surface of a circular, tensile silicon nitride diaphragm. Several devices were tested for linearity, frequency response, drift, noise, and power. The sensors exhibit a Sound Pressure Level (SPL) response characterized by a noise floor of 52 dB, linearity up to 160 dB, and power con-

* Corresponding author. Tel.: +1 614 688 3689.
E-mail address: dapino.1@osu.edu (M.J. Dapino).

0924-4247/$ – see front matter © 2009 Elsevier B.V. All rights reserved.
doi:10.1016/j.sna.2009.04.008

sumption of 15 mW when operated at 3 V. Horowitz at al. [2] developed a micromachined piezoelectric microphone for aeroacoustic measurement applications. The microphone was fabricated by combining a lead zirconate–titanate (PZT) deposition process on a silicon-on-insulator wafer with deep reactive ion-etching. An experimental setup in a plane-wave tube was used to characterize the microphone. The device exhibits a sensitivity of 0.75 μV/Pa, a dynamic range of 47.8–169 dB and a resonance frequency of 50.8 kHz. Wang et al. [7] built a PZT-based microacoustic sensor that employs interdigitated electrodes and in-plane polarization instead of commonly used parallel plate-electrodes and through-thickness polarization. The sensitivity is greatly improved because of the small capacitance of the interdigitated capacitor and the large and adjustable electrode spacing, as well as the advantage of the relatively larger piezoelectric stress constant g_{33}.

The piezoelectricity of Polyvinylidene Fluoride (PVDF), first observed by Kawai [8], has been widely used for sensor development in a wide range of military, industrial and biomedical applications. PVDF can generate voltages 10–25 times higher than piezoceramics for the same pressure input. These polymers are quite stable because they can resist moisture, most chemicals, oxidants and intense ultraviolet and nuclear radiation. PVDF is synthesized by addition polymerization of the CH2=CF2 monomer, and exhibits α, β, γ and δ phases. The α phase is non-piezoelectric. The γ and δ phases are not common. The β phase form, which has a net dipole moment pointing from the electronegative fluorine to the electropositive hydrogen, produces a net dipole moment nearly normal to the polymer chain [9]. Defect groups of head to head and tail to tail are believed to be responsible for the formation of β phase and hence for the piezoelectric properties [10].

Sensors based on PVDF film are attractive due to their high sensitivity and low cost. For example, a PVDF film pressure sensor is used for in-sleep cardiorespiratory monitoring [11]. Uncooled infrared (IR) sensors using PVDF thin film are used to detect temperature changes from low levels of incident IR radiation [12]. Wang et al. [13] developed a PVDF sensor array for measurement of the impulsive pressure generated by cavitation induced by bubble collapse. A laser micromachining technique was used to fabricate the PVDF sensor array and each sensor has a sensing area of 4.8 mm × 4.8 mm and a height of 25 μm. The capacitance is determined by overlapping isolated electrodes from both sides, which forms the sensing area. It was shown that this sensor can measure gas dynamic shock as fast as 31 ns, while measurements of impact signals from a dropping ball show an insignificant crosstalk level of less than 2%.

The voltage produced by a capacitive sensor is given by the ratio between charge and capacitance. The proposed microphone exploits the key advantages of PVDF as a sensor material by means of two key design elements aimed at increasing the charge and decreasing the effective device capacitance (Fig. 1). The first design element is a stress amplification mechanism through the area ratio between the overall surface exposed to acoustic waves and the area of the individual micro-pillars. Because PVDF responds to stress, this mechanism increases the amount of charge for a given pressure level. A rigid membrane placed between the micro-pillars and the acoustic medium ensures high mechanical coupling. The second design element is a top electrode patterned to cover only the surface of the micro-pillars. The design with patterned electrodes reduces the capacitance of the sensor by excluding the capacitance of the air between micro-pillars. The individual round electrodes above each micro-pillar are interconnected by means of thin conducting tabs. A continuous, flat electrode is placed underneath the array.

The sensitivity of the proposed microphone is analyzed in Section 2 and compared against the sensitivity of flat continuous PVDF film and micro-pillars with full flat electrodes. The optimization algorithm for minimization of the microphone's footprint is presented in Section 3. Details on the fabrication of the micro-pillars and characterization experiments aimed at understanding the coupled electromechanical response of the PVDF micro-pillars are presented in Section 4.

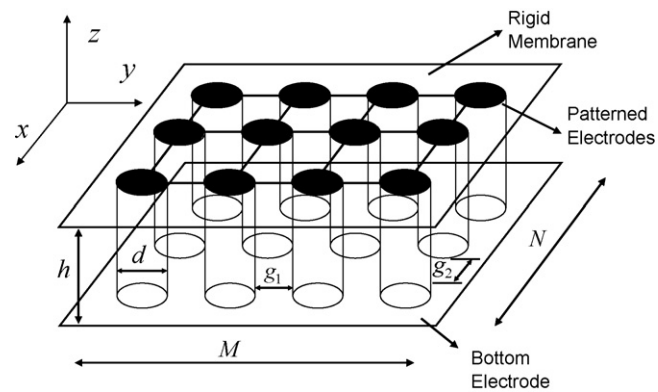

Fig. 1. Schematic diagram of the proposed acoustic pressure sensor based on PVDF micro-pillars and patterned electrodes. A rigid membrane placed above the micro-pillar array acts as a pressure amplifier. The patterned electrode reduces the device capacitance, thus increasing its sensitivity.

2. Sensitivity analysis

The static sensitivity is defined as the ratio of the output voltage over the stress acting on the PVDF material,

$$K = V_o/\sigma. \tag{1}$$

The sensitivities of three PVDF sensor designs are compared: flat continuous film, micro-pillars with full electrodes, and micro-pillars with patterned electrodes.

2.1. Flat continuous PVDF film

Fig. 2 shows the open circuit of a flat PVDF film sensor. According to the linear piezoelectric constitutive equations, the open circuit voltage developed across the film thickness is

$$V_o = -g_{33} \cdot \sigma \cdot h, \tag{2}$$

where g_{33} is the piezoelectric stress constant in the x_3-direction, $\sigma = P$ is the applied acoustic pressure, and h is the thickness of the PVDF film. In this case, the stress induced in the material is equal to the pressure. Substitution of Eq. (2) into (1) gives the sensitivity as

$$K_1 = -g_{33} \cdot h. \tag{3}$$

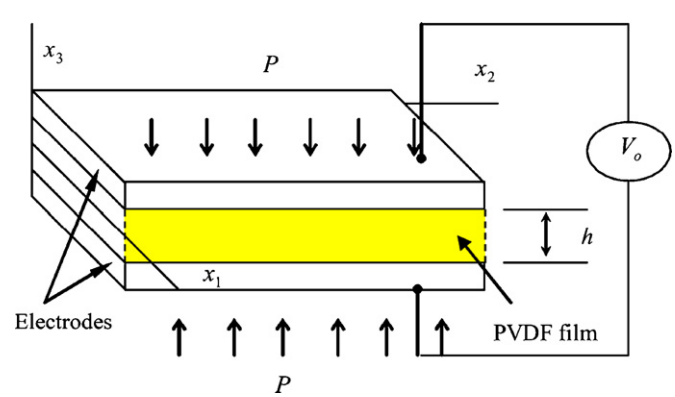

Fig. 2. PVDF film open circuit.

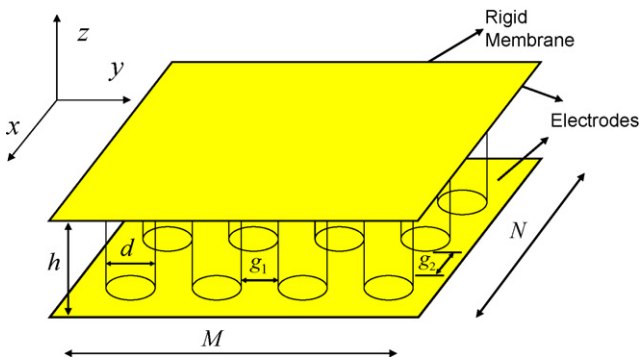

Fig. 3. Schematic diagram of PVDF micro-pillar sensor with full electrodes.

2.2. PVDF micro-pillars with full electrodes

Fig. 3 illustrates the case when an array of micro-pillars is placed between two continuous, flat electrodes. The charge output by the sensor corresponds to the charge generated by the micro-pillars,

$$Q = Q_p \equiv C_p \cdot V_p, \tag{4}$$

where Q is the total charge collected at the electrodes, Q_p is the charge generated by the micro-pillars, C_p is the total capacitance of the micro-pillars, and V_p is the potential across the micro-pillars. The total capacitance is, by definition,

$$C_p \equiv \varepsilon \cdot \frac{A}{h} = \varepsilon \cdot \frac{M \cdot N \cdot \pi/4 \cdot d^2}{h}, \tag{5}$$

where ε is permittivity of PVDF, M is number of pillars in the x-direction, N is number of pillars in the y-direction, A is the total cross-sectional area of the micro-pillars, and d is the diameter of each micro-pillar. The voltage across the micro-pillars is proportional to the stress,

$$V_p = -g_{33} \cdot h \cdot \sigma. \tag{6}$$

The stress on each pillar due to the application of normal pressure on the sensor surface is

$$\sigma = \frac{(d+g_1)\cdot(d+g_2)}{\pi d^2/4} \cdot P, \tag{7}$$

where g_1 is the gap between pillars in the x-direction and g_2 is the gap between pillars in the y-direction. Substitution of (7) into (6) gives

$$V_p = -g_{33} \cdot h \cdot \frac{(d+g_1)\cdot(d+g_2)}{\pi d^2/4} \cdot P. \tag{8}$$

The total capacitance is the sum of the capacitance of the micro-pillars and the capacitance of the air gap,

$$C_t = C_p + C_o, \tag{9}$$

in which the air capacitance is

$$C_o = \varepsilon_o \cdot \frac{M \cdot N \cdot [(d+g_1)(d+g_2) - \pi d^2/4]}{h}. \tag{10}$$

Since the two capacitances are connected in parallel, the voltage drop is the same across the micro-pillars and air gap,

$$V_o = V_p = \frac{Q}{C_t}. \tag{11}$$

Combination of Eqs. (4), (5) and (8)–(11) gives the sensitivity of PVDF micro-pillars with full electrodes as

$$K_2 = \frac{\varepsilon_r (d+g_1)(d+g_2)}{\pi d^2/4 \cdot (\varepsilon_r - 1) + (d+g_1)(d+g_2)} \cdot (-g_{33} \cdot h), \tag{12}$$

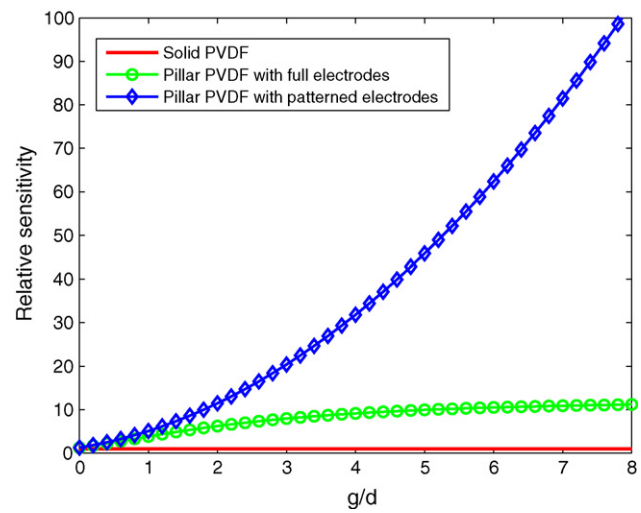

Fig. 4. Relative sensitivity of the proposed PVDF micro-pillar sensor with patterned electrodes compared to PVDF film and fully electroded micro-pillars. The gaps are assumed equal ($g = g_1 = g_2$).

where ε_r is the relative permittivity of PVDF. Assuming without losing generality that $g_1 = g_2 = g$, the sensitivity of the micro-pillar array based on full electrodes relative to the sensitivity of solid PVDF film is

$$K_{r2} \equiv \frac{K_2}{K_1} = \frac{\varepsilon_r (1+g/d)^2}{\pi/4 \cdot (\varepsilon_r - 1) + (1+g/d)^2}. \tag{13}$$

The relative sensitivity of the micro-pillar sensor is limited by the relative permittivity of PVDF film, and the upper bound is $K_{r2} = \varepsilon_r$ as g/d goes to infinity.

2.3. PVDF micro-pillars with patterned electrodes

In this case both the capacitance and the charge are due solely to the micro-pillars, hence the sensitivity has the form

$$K_3 = \frac{(d+g_1)\cdot(d+g_2)}{\pi d^2/4} \cdot (-g_{33} \cdot h). \tag{14}$$

Assuming as before $g_1 = g_2 = g$, the sensitivity of the pillar sensors based on patterned electrodes relative to the sensitivity of PVDF film is

$$K_{r3} \equiv \frac{K_3}{K_1} = \frac{(1+g/d)^2}{\pi/4}, \tag{15}$$

which increases monotonically with the ratio of the gap between pillars and the pillar diameter, g/d. The effect of the air gap between pillars is to increase the stress on the sensing material and therefore to increase the sensor's output voltage and sensitivity.

A comparison of the sensitivities of the two micro-pillar designs relative to that of solid PVDF film is shown in Fig. 4. The micro-pillar sensor with patterned electrodes theoretically has an unlimited sensitivity with increasing geometry ratio g/d (assuming $g = g_1 = g_2$).

To simplify the design of the micro-pillars with patterned electrodes, we assume that the width of the connecting tabs is negligible compared with the diameter of the micro-pillars. The smallest tab width allowed by our current fabrication techniques (Section 4) is about 2 μm. If the diameter of micro-pillars is not high enough, this factor needs to be included in the calculation of sensitivity.

3. Optimization

Nonlinear programming (NLP) techniques are used to find a minimum or maximum of an objective function in N_d dimensions which satisfies arbitrary complex constraints [14]. Many algorithms have been developed for solving such problems. We utilize an algorithm based on the interior-reflective Newton method described in [15]. Each iteration involves the approximate solution of a large linear system using the method of preconditioned conjugate gradients (PCG). The optimization problem can be expressed in the form

$$\begin{cases} \text{minimize} & f(x) \\ h_i(x) \le 0 & i = 1, \ldots, m \\ g_i(x) = 0 & i = 1, \ldots, k \\ l_i \le x_j \le u_j & j = 1, \ldots, n. \end{cases} \tag{16}$$

Here, x is an N_d-dimensional list of design variables; $f(x)$ is the objective function; $h_i(x)$ are inequality constraints; $g_i(x)$ are equality constraints; and $l_i \le x_j \le u_j$ are constraints for all design variables.

The functions $f(x)$, $h_i(x)$ and $g_i(x)$ can be any linear or nonlinear combination of the design variables. In this case, a constrained NLP optimization algorithm was developed to obtain the sensor's geometric parameters (M, N, d, g_1, g_2 and h) needed to achieve 100× the sensitivity of existing commercial sensors, dynamic range up to 181 dB, and frequency bandwidth of 100 kHz. The objective function to be minimized is the total sensor area,

$$f(x) = M \cdot N \cdot (d + g_1) \cdot (d + g_2). \tag{17}$$

The NLP optimization algorithm was implemented in Matlab.

The design variables that were optimized are M, N, d, g_1, g_2, h and R (total input resistance of the amplifier). The design variables can be treated as independent of one another, while the dependent variables are related by the equality constraints. The total input resistance of the amplifier cannot be chosen arbitrarily as it depends on the actual specifications of available operational amplifiers, although it usually is very high. The height of the pillars is dictated by manufacturing constraints and usually takes values such as 10 μm or 20 μm.

Bounds on the design variables are affected by the ability of the manufacturing process and amplifier input resistance. For this case, they are defined by

$$\begin{cases} 1 \le M \le 200 \\ 1 \le N \le 200 \\ 1\,\mu\text{m} \le d \le 1000\,\mu\text{m} \\ 1\,\mu\text{m} \le g_1 \le 1000\,\mu\text{m} \\ 1\,\mu\text{m} \le g_2 \le 1000\,\mu\text{m} \\ 1\,\mu\text{m} \le h \le 500\,\mu\text{m} \\ 100\,\text{M}\Omega \le R \le 1\,\text{T}\Omega. \end{cases} \tag{18}$$

The theory presented here incorporates no mechanisms to account for edge effects, though in practice the electrode edges may induce field leakage. In the limit when there is only one pillar ($M = N = 1$), the sensor can still be conceived so long as g_1 and g_2 are defined. In this case, the gaps between pillars do not exist as such but they can be defined at the edge of the sensor. In practice, the number of pillars in each direction must be much bigger than one to minimize edge effects. The determination of geometric parameters that satisfy the various design constraints is presented next.

3.1. Resonance frequency

The basic sensing element, i.e., a PVDF micro-pillar, can be modeled as a continuous rod fixed at one end and free at the other end, as shown in Fig. 5. Assuming a slender rod and ignoring inertias and electromechanical coupling, the governing equation for the longitudinal vibrations of a rod is a partial differential equation [16]

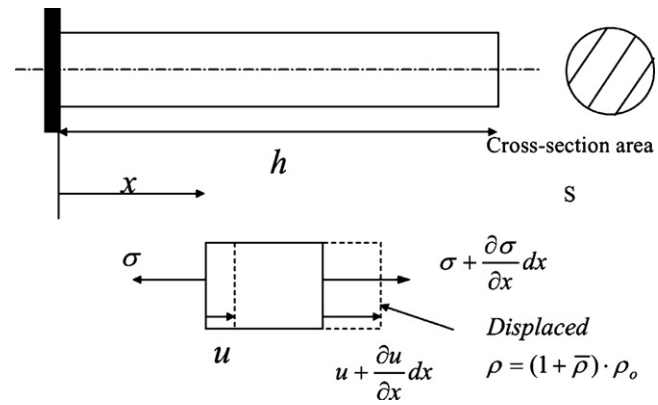

Fig. 5. Schematic of a continuum rod model.

$$\frac{\partial^2 u}{\partial x^2} - \frac{1}{c^2}\frac{\partial^2 u}{\partial t^2} = 0, \tag{19}$$

where u denotes the axial displacement at position x and time t, and $c = E/\rho_0$, where E and ρ_0 are the Young's modulus and mass density of the material, respectively. Considering fixed-free boundary conditions, the natural frequencies of Eq. (19) have the form [17]

$$\omega_r = \frac{(2r-1)\pi}{2h}\sqrt{\frac{E}{\rho_0}}, \quad r = 1, 2, 3, \ldots \tag{20}$$

A PVDF rod can be modeled as a system comprising a second-order mechanical system (Fig. 6(a)) and a first-order electrical

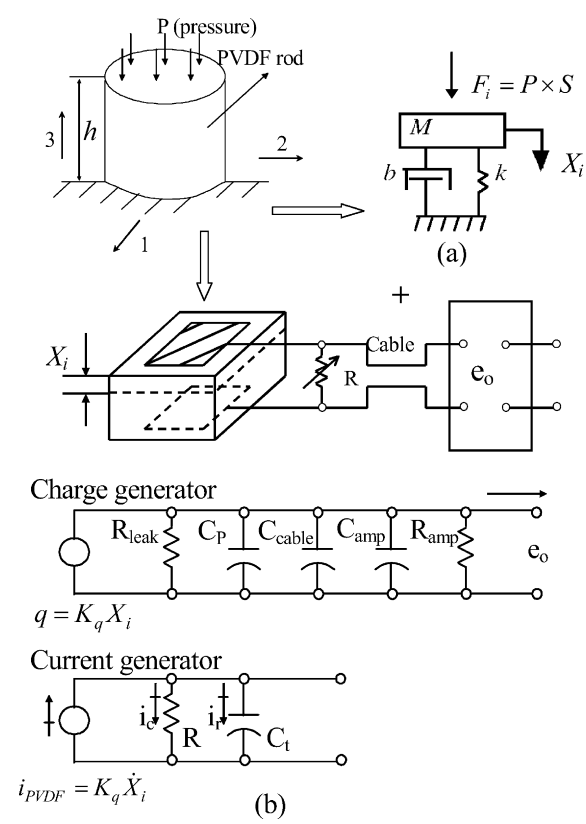

Fig. 6. PVDF rod model and equivalent circuit. (a) Second-order mechanical representation of a micro-pillar array. (b) First-order electrical representation of the sensor system.

system (Fig. 6(b)). The system transfer function is expressed by

$$\frac{E_o(s)}{F_i(s)} = \frac{G_1 \tau s}{\tau s + 1}\left[\frac{G_2}{((1/\omega_n^2)s^2) + ((2\xi/\omega_n)s + 1)}\right], \tag{21}$$

in which τ is the time constant of the first-order system, ω_n is the natural frequency of the second-order system, ξ is damping ratio, and G_1 and G_2 are the gains of the first order system and second-order system, respectively.

The frequency response associated with Eq. (21) is shown in Fig. 7. If the sensor is operated in the flat magnitude range of the frequency response function and the passband error is ±5%, the bandwidth of the system will be from $3/\tau$ to $\omega_n/5$. The desired frequency bandwidth of the acoustic sensor is 20 Hz to 100 kHz, which implies

$$\omega_n/5 \geq 100 \times 10^3 \times (2\pi). \tag{22}$$

From Eq. (20), the first natural frequency of the PVDF rod (let $r = 1$) is

$$\omega_n = \frac{\pi}{2h}\sqrt{\frac{E}{\rho_0}}. \tag{23}$$

Substitution of Eq. (23) into Eq. (22) and solution for h gives,

$$h \leq 530\,\mu\text{m}, \tag{24}$$

which represents the natural frequency constraint.

3.2. Cutoff frequency

According to Fig. 7 and the bandwidth requirement, the cutoff frequency constraint is

$$3/\tau \leq 20 \times (2\pi). \tag{25}$$

From Fig. 6(b), the time constant is $\tau = RC_t$. For the case of micro-pillars with patterned electrodes, the total capacitance of the system is the capacitance of the pillars (note that the capacitance of the cable and the amplifier is relatively small compared to the capacitance of the pillars), so that $C_t = C_p$. Combining Eqs. (5) and (25), one obtains the cutoff frequency constraint,

$$\frac{3h}{R \cdot M \cdot N \cdot \varepsilon \cdot \pi d^2/4} - 40\pi \leq 0. \tag{26}$$

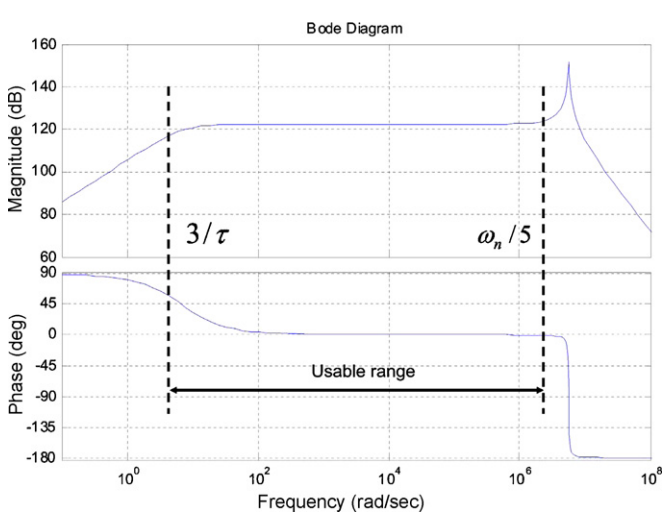

Fig. 7. Bode plot associated with the electromechanical system shown in Fig. 6.

3.3. Dimensional limits in the x and y directions

The acoustic sensor is designed to be packaged in a 9 mm^2 enclosure, which requires that the dimensions in the x and y directions cannot be greater than 3 mm. The dimensional constraints in the x and y directions thus are:

$$M \cdot (d + g_1) - 3 \times 10^{-3} \leq 0, \tag{27}$$

$$N \cdot (d + g_2) - 3 \times 10^{-3} \leq 0. \tag{28}$$

3.4. Sensitivity

Based on the specifications of existing commercial products, the acoustic sensor must have a sensitivity of no less than 0.3 V/psi, i.e., 4.35×10^{-5} V/Pa, before amplification. A gain of 1000 would increase the sensitivity to about the same level as the most sensitive commercial microphones. According to Eq. (14), the sensitivity constraint has the form

$$4.35 \times 10^{-5} - (-g_{33}) \cdot \frac{(d + g_1)(d + g_2)}{\pi d^2/4} \cdot h \leq 0. \tag{29}$$

3.5. Yield strength

If the sensor is assumed to have a pressure limit equivalent to a sound pressure level of 181 dB, the maximum allowable acoustic pressure ($P_{\max}$) is given by

$$20 \log\left(\frac{P_{\max}}{20 \cdot 10^{-6}}\right) = 181\,\text{dB}. \tag{30}$$

The constraint to avoid surpassing the yield strength of PVDF is

$$P_{\max} \cdot \frac{(d + g_1)(d + g_2)}{\pi d^2/4} \leq \sigma_Y \tag{31}$$

where σ_Y is the yield strength.

3.6. Buckling load

The Euler formula for columns is

$$F_{\max} = \frac{\pi^2 EI}{(rh)^2}, \tag{32}$$

where $F_{\max}$ is the maximum or critical force (vertical load on a column), E is modulus of elasticity, I is area moment of inertia, h is unsupported length of column, and r is column effective length factor. For both ends pinned, $r = 1.0$; for both ends fixed, $r = 0.50$; for one end fixed and the other end pinned, $r = 0.70$; for one end fixed and the other end free to move laterally, $r = 2.0$. For the micro-pillar sensor, the buckling load condition is

$$P_{\max}(d + g_1)(d + g_2) \leq F_{\max}. \tag{33}$$

Substitution of Eq. (32) into Eq. (33) and consideration of the area moment of inertia of a round pillar gives,

$$P_{\max}(d + g_1)(d + g_2) - \frac{\pi^2 \cdot E \cdot \pi d^2/4}{(r \cdot h)^2} \leq 0. \tag{34}$$

Figs. 8–11 show design curves calculated with the optimization procedure described above. Specifically, the figures show calculations of pillar diameter, pillar gap, g/d ratio and aspect ratio versus pillar height based on various practical amplifier input resistances ranging from 1 G Ω to 1000 G Ω. These plots provide information on the selection of the amplifier input resistances and the pillar height and diameter. Fig. 8 shows that for $R \leq 10$ G Ω the calculated optimal pillar diameter monotonically increases with pillar height. For higher input resistance values the optimal pillar diameter is approximately constant (2–4 μm), i.e., it is approximately

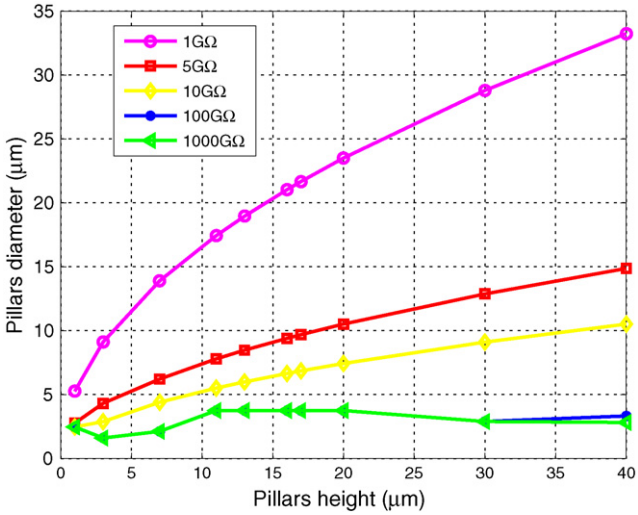

Fig. 8. Optimal pillar diameter versus pillar height as a function of amplifier input resistance.

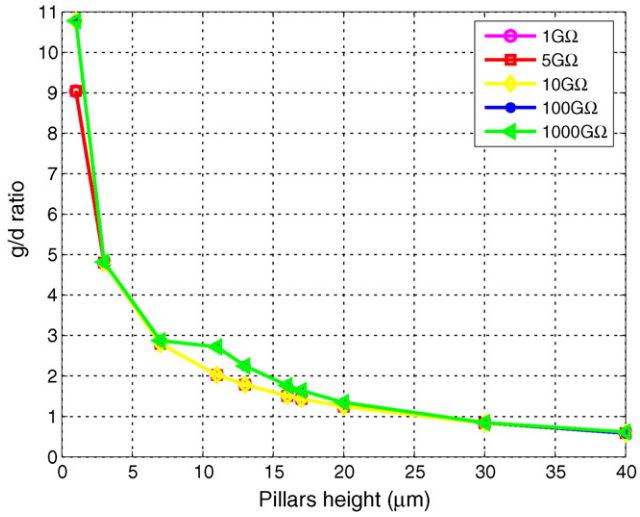

Fig. 9. Optimal g/d ratio versus pillar height as a function of amplifier input resistance.

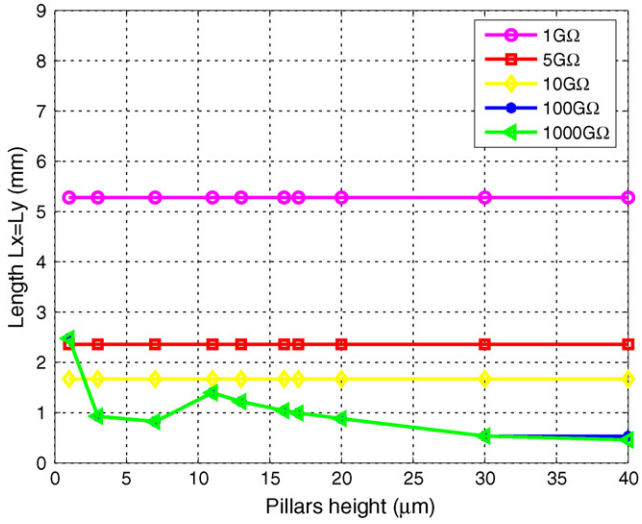

Fig. 10. Optimal length versus pillar height as a function of amplifier input resistance.

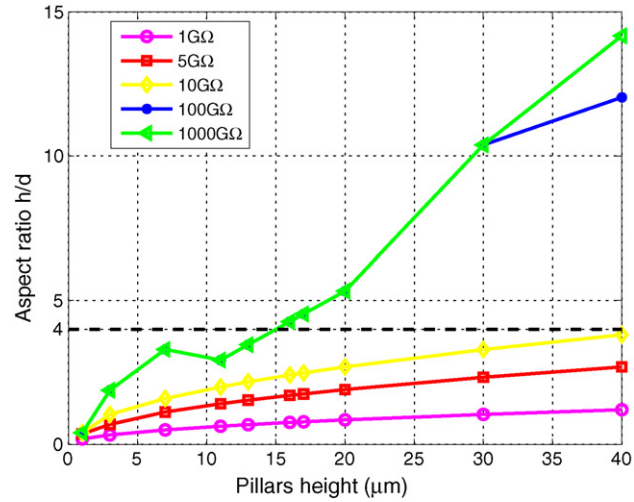

Fig. 11. Optimal aspect ratio versus pillar height as a function of amplifier input resistance.

independent of pillar height. Fig. 9 shows that the optimal g/d ratio monotonically decreases with pillar height. Fig. 10 shows that if the amplifier input resistance is $R \geq 100\,\mathrm{G}\,\Omega$, an overall sensor footprint of less than 1 mm^2 can be achieved. According to Fig. 11, if aspect ratios of $g/d = 4$ could be manufactured as is expected to be the case in the near future, any amplifier input resistance from 1 G Ω to 10 G Ω would be suitable. The pillar height should be less than 15 μm if the amplifier input resistance was greater than 100 G Ω. A limit on the pillar ratio of 2 implies either $R = 1\,\mathrm{G}\,\Omega$ combined with arbitrary pillar heights or increasingly higher input resistances combined with increasingly lower pillar heights.

4. Fabrication and characterization of electroactive PVDF micro-structures

Polyvinylidene fluoride (PVDF) micro-structures were fabricated using a procedure which is described in detail elsewhere [18]. Previously patterned polydimethylsiloxane (PDMS) stamps molded from photolithographically fabricated masters were used to obtain arrays of PVDF micro-pillars with designed dimensions (Fig. 12(a)). A 10% PVDF solution in dimethylacetamide/acetone was spin coated on the PDMS stamps at 1000–2000 rpm for 1 min. The stamps were placed on a hot plate at 100 ° C for 5 min in order to drive off residual solvent and anneal the PVDF. The spin coated PVDF film was then transferred onto the adhesive side of copper tape using slight pressure. Fig. 12(b) and (c) shows scanning electron micrographs of PVDF pillars with two different micro-pillar dimensions.

Preliminary experiments were conducted with the goal to characterize the piezoelectric response of the PVDF micro-pillars. These proof-of-concept experiments were conducted on a non-optimal micro-pillar array ($d = 5\,\mu\mathrm{m}$, $g = 5\,\mu\mathrm{m}$, $h = 6\,\mu\mathrm{m}$, $N = M = 1000$). A gold-coated glass slide was placed on top of the micro-pillars (top electrode), and an electric field of ∼120 MV/m was applied across the electrodes (top positive and bottom negative) at 160 ° C for 3 h, and then at room temperature for an additional hour to pole the PVDF micro-structures. The direct and inverse piezoelectric responses were characterized using a Hysitron TriboIndenter nano-mechanical test instrument equipped with the nanoECR package (Fig. 13) [19]. A boron-doped diamond 14.5 μm flat punch indenter probe was used in the experiments.

The inverse piezoelectric effect was tested by measuring the displacement of a micro-pillar when it is subjected to simultaneous force and voltage inputs. Running the instrument in load-control mode to ensure that a constant preload force of 3 μN was preserved

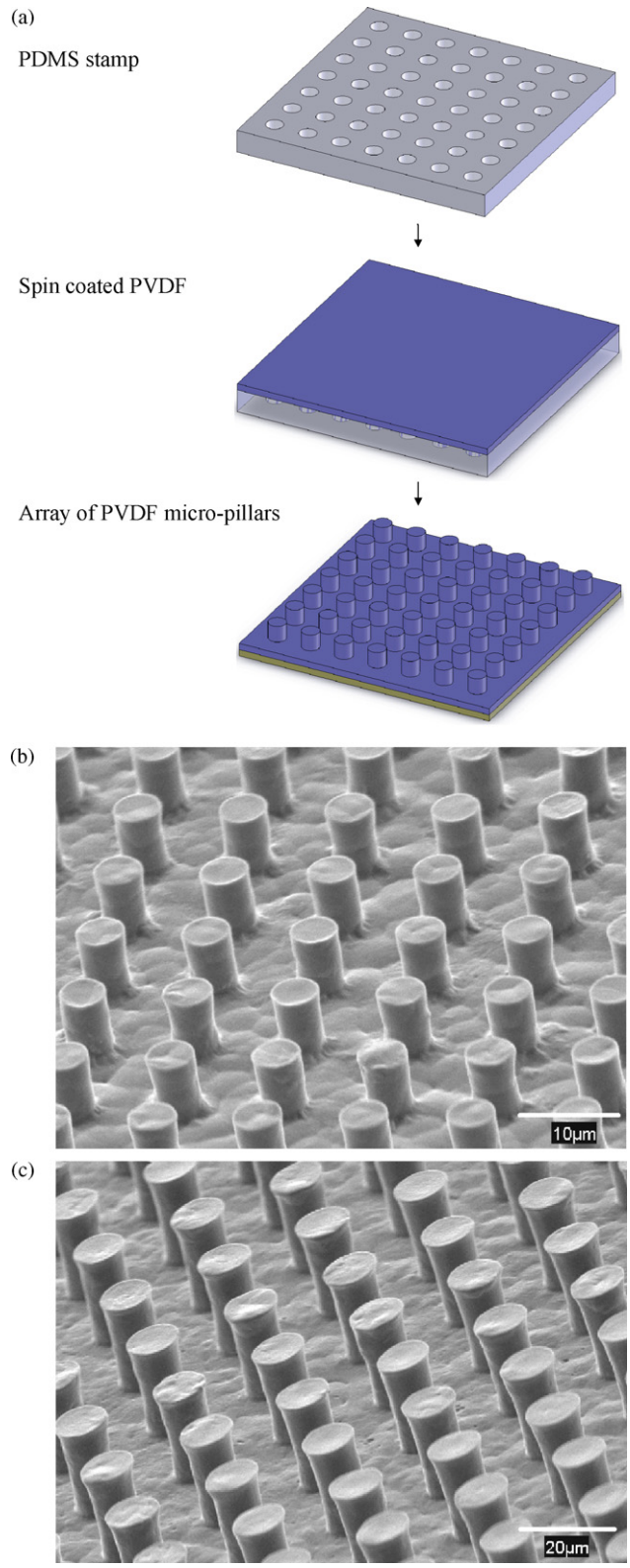

Fig. 12. (a) Fabrication schematic of PVDF micro-pillars. SEM micrograph of (b) ~ 5 ×5 μm pillars and (c) ~ 10 ×20 μm pillars (bottom).

throughout the test, a 40 V pulse was applied across the electrodes. The preload was gradually applied on a pillar from $t = 0$–5 s and maintained for 60 additional seconds as shown in Fig. 14(a). The 40 V pulse was applied for 5 s intervals at $t = 35$, 45, and 55 s, as shown in Fig. 14(b). The sample was subjected to a preload to

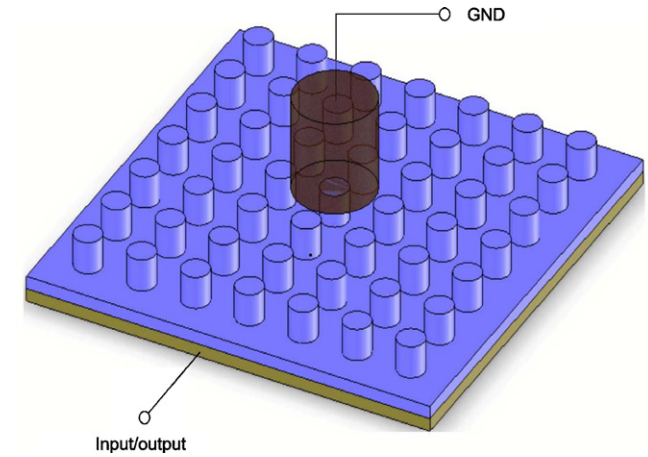

Fig. 13. Schematic of the indentation test conducted with a nano-mechanical test instrument.

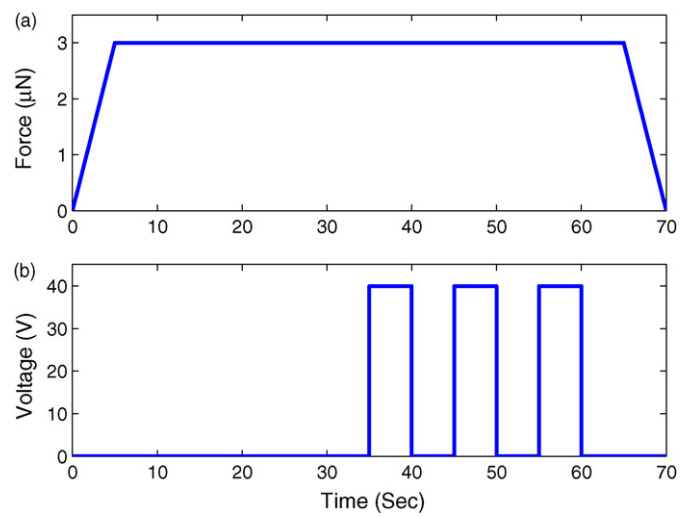

Fig. 14. Load-controlled nano-indentation inputs of (a) 3 μN force and (b) 40 V square wave.

ensure a good flat contact between the tip of the instrument and the top of the pillar before starting each test. As shown in Fig. 12(b), the top surface of the PVDF pillars is not completely flat, due in part to the crystalline nature of the polymer. Fig. 15 shows displacement versus time results. The five lines correspond to five

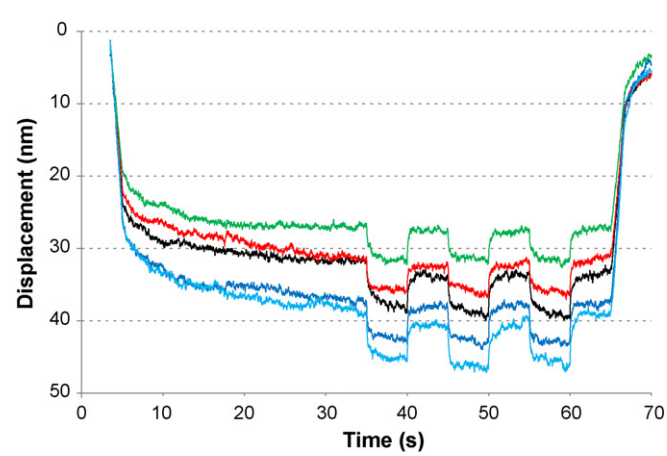

Fig. 15. Plot of displacement versus time from the 40 V square wave tests.

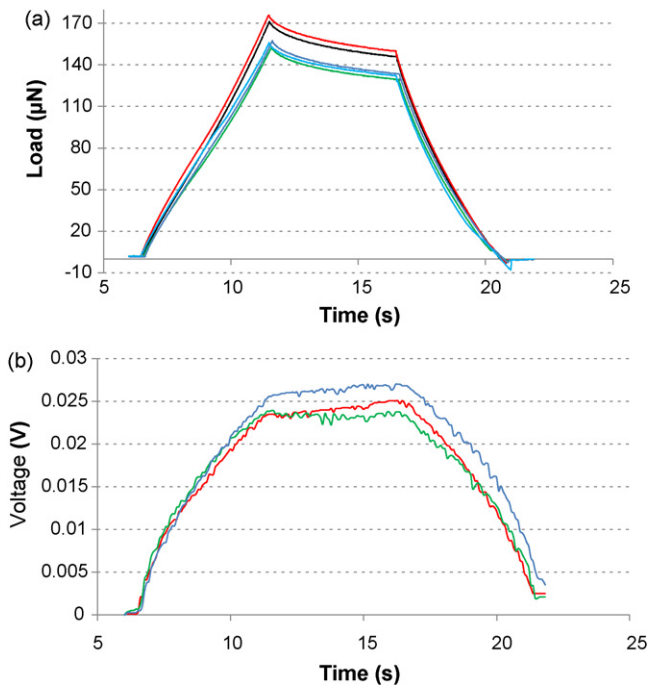

Fig. 16. Plots of (a) force versus time and (b) voltage versus time for the 4 μm displacement-controlled indents.

different tests conducted on the same sample. There are two distinct sets of lines, which correspond to two separate sets of tests (conducted 4 days apart). We note that the static displacement differs by about 10 nm for the five measurements. This difference is insignificant considering the dimensions of the pillars (5000 nm). What is important is that the relative change in displacement caused by the 40 V input was very consistent for all five tests. The curves show an average displacement change of approximately 4.4 ± 0.56 nm (strain of ~0.001) with the applied 40 V pulse. The direct piezoelectric effect was tested by measuring the voltage generated by a micro-pillar in displacement-controlled nano-indentation tests. Fig. 16 shows force and voltage versus time results. A voltage of roughly 0.025 ± 0.0026 V was generated during each test. A total of 5 measurements (represented by 5 different lines) were taken in both characterizations. The results confirm a piezoelectric response of the PVDF micro-pillars under an applied voltage or mechanical input.

The piezoelectric constants d_{33} and g_{33} estimated from the data are −110 pC/N and −1092 mV/m/N, respectively [20]. These two values are nearly 3 times greater than those typically reported for flat PVDF films, approximately −33 pC/N and −330 mVm/N, respectively [21]. The high values of these coefficients are consistent with results obtained from micro-fabricated PVDF from AFM results reported in the literature [22,23]. The large coefficients could be attributed to several factors including potential effects of micro-structure and electrode geometry and expected differences in mechanical compliance between the PVDF micro-pillars and flat PVDF. The micro-pillars are subjected to lower mechanical loading as they are not constrained by surrounding material, hence they are expected to deform more than solid film for a given electric field input [24].

5. Discussion and future work

Micro-electromechanical MEMS technology has traditionally been focused on silicon based fabrication techniques. With the development of sacrificial layer micro-molding (SLaM) and patterned substrate micro-molding (PSM), the micro-fabrication of polymer micro-structures is becoming increasingly promising [25,26]. An acoustic sensor with small size, high sensitivity, wide dynamic range and high frequency bandwidth is of great need due to the special requirements of aeroacoustic and clinical applications. The small size, high stiffness, and reduced mass of MEMS sensors are of great interest because such devices can significantly improve both the temporal and spatial measurement bandwidth. This article presents the design, theoretical analysis, micro-fabrication and proof-of-concept characterization of a new type of millimeter-size acoustic sensor using PVDF micro-pillars and patterned electrodes, with the potential to achieve 100× the sensitivity of existing commercial sensors in combination with a dynamic range of 181 dB and a frequency bandwidth of at least 100 kHz. A constrained optimization algorithm has been developed as a function of geometric parameters and electrical parameters of the sensor and conditioning amplifier. A micro-fabrication process based on PVDF micro-pillars and patterned electrodes is described. In order to determine the piezoelectric properties, a PVDF sample that consists of a uniform pattern of 5 μm pillars was manufactured and tested on a Hysitron TriboIndenter nano-mechanical test instrument. The nano-indentation testing results show that the PVDF micro-pillar sample exhibits obvious piezoelectric responses under an applied voltage or strain.

One potential application of the proposed micro-acoustic sensor would be vehicle positioning. Like animal echolocation, the vehicle would emit ultrasonic waves and an array of micro-sensors placed on the vehicle skin would measure in real time the echo of the emission (both magnitude and direction). The time difference between the emitted and reflected waves would provide localization of objects around the vehicle and would create safer driving conditions. Spatial location requires pointpoint accuracy, hence sensor dimensions much smaller than possible to fabricate with conventional designs.

Optimal sensor manufacturing and testing is out of the scope of this paper and will be addressed in future work. Future work will be focused on the fabrication of optimal micro-pillar sensors, amplifier circuit design for the device and acoustic tests. Specialized amplifier circuit design is crucial for acoustic tests of the micro-acoustic sensor. There are three amplifier options for this application: DC coupled amplifier, AC coupled amplifier and DC servo loop amplifier. The advantages and disadvantages of the three amplifier designs will be analyzed. Frequency response analysis, sensitivity calibration, linearity measurement and power spectrum analysis will also be investigated.

The preamplifier circuit is very important for the signal conditioning of the PVDF sensor based on micro-pillars and patterned electrodes. There are two types of integrated circuits generally used in piezoelectric sensors: charge and voltage amplifiers. For the charge amplifiers, the output voltage is equal to Q/C_f (where C_f is the capacitance of the feedback capacitor), which means that the output voltage is independent of the sensor capacitance. Using a small C_f can lead to a very large voltage output. However, it is impractical to use charge amplified systems above 50 kHz since the feedback capacitor exhibits filtering characteristics above this range. Therefore, the voltage amplifier is employed in our circuit design. A PVDF microphone behaves as a capacitor, hence it generates output voltages with a high impedance level. The source impedance combined with the load resistance provided by the amplifier generates a voltage divider. As the ratio of the load resistance to the source impedance decreases, the output voltage also decreases, which is known as the loading effect. This issue can be addressed by a buffer circuit using an operational amplifier such as the Analog Devices AD7xx. This amplifier has very high input resistance (from 2 G Ω to 300 G Ω) and small output resistance (around 10 Ω). The buffer circuit converts the high output impedance of

the microphone into a low impedance signal which eliminates the loading effect and thus minimizes the signal loss.

Acknowledgements

J.X. and M.J.D. acknowledge the member organizations of the Smart Vehicle Concepts Center (www.SmartVehicleCenter.org) and the National Science Foundation Industry/University Cooperative Research Centers program (www.nsf.gov/eng/iip/iucrc) for supporting this work. Support for D.G.P. and D.H. comes from AFOSR MURI #F49620-03-1-0421. We acknowledge Ryan Stromberg and Rick Nay of Hysitron Inc. for assistance with the indentation tests and OSU Nanotech West Lab technical staff for technical assistance. The authors are thankful to Kenneth Cunefare for useful discussions.

References

[1] D. Arnold, S. Gururaj, S. Bhardwaj, T. Nishida, M. Sheplak, A piezoresitive microphone for aeroacoustic measurements, in: Proc. ASME International Mechanical Engineering Congress and Exposition, New York, NY, 2001.
[2] S. Horowitz, T. Nishida, T. Nishida, M. Sheplak, Design and characterization of a micromachined piezoelectric microphone, in: Proc. 26th AIAA Aeroacoustics Conference, Monterey, CA, 2005.
[3] S. Charleston-Villalobos, S. Cortes-Rubiano, R. Gonzalez-Camarena, G. Chi-Lem, T. Aljama-Corrales, Respiratory acoustic thoracic imaging (RATHI): Assessing deterministic interpolation techniques, Med. Biol. Eng. Comput. 42 (2004) 618–626.
[4] R. Murphy, Method and apparatus for displaying body sounds and performing diagnosis based on body sound analysis, U.S. Patent No. 6,790,183 (2004).
[5] K. Grosh, J. Zheng, E. deBoer, A.L. Nuttall, High frequency electromotility of the cochlea, J. Acoust. Soc. Am. 115 (2004) 2178–2184.
[6] R.D. White, K. Grosh, Microengineered hydrodynamical cochlear model, Proc. Natl. Acad. Sci. 102 (2005) 1296–1301.
[7] C. Wang, Z. Wang, L. Liu, Design and analysis of a PZT-based micromachined acoustic sensor with increased sensitivity, IEEE Trans. Ultrason. Ferroelectr. 52 (2005) 1840–1850.
[8] H. Kawai, The piezoelectricity of poly (vinylidene fluoride), JPN. J. Appl. Phys. 8 (1979) 975–976.
[9] M. Ramos, H. Correia, S. Lanceros-Mendez, Atomistic modelling of processes involved in poling of PVDF, Comp. Mater. Sci. 33 (2005) 230–236.
[10] T. Dargaville, M. Celina, J. Elliott, P. Chaplya, G. Jones, D. Mowery, R. Assink, R. Clough, J. Martin, Characterization, performance and optimization of PVDF as a piezoelectric film for advanced space mirror concepts, Tech. Re SAND2005–6846, Sandia National Laboratories, 2005.
[11] F. Wang, M. Tanaka, S. Chonan, Development of a PVDF piezopolymer sensor for unconstrained in-sleep cardiorespiratory monitoring, J. Intell. Mater. Syst. Struct. 14 (2003) 185–190.
[12] N. Fujitsuka, J. Sakata, Y. Miyachi, K. Mizuno, K. Ohtsuka, Y. Taga, O. Tabata, Monolithic pyroelectric infrared image sensor using PVDF thin film, Sens. Actuators A 66 (1998) 237–243.
[13] Y. Wang, C. Huang, Y. Lee, H. Tsai, Development of a PVDF sensor array for measurement of the impulsive pressure generated by cavitation bubble collapse, Exp. Fluids 41 (2006) 365–373.
[14] P. Gill, M. Murray, M. Wright, Practical Optimization, Academic Press, London, 1981.
[15] T. Coleman, Y. Li, An interior, trust region approach for nonlinear minimization subject to bounds, SIAM J. Optim. 6 (1996) 418–445.
[16] D. Inman, Engineering Vibration, Prentice-Hall, NJ, 2001.
[17] R.D. Blevins, Formulas for Natural Frequency and Mode Shape, Van Nostrand Reinhold Co, New York, NY, 1979.
[18] D. Gallego-Perez, N. Ferrell, N. Higuita, D. Hansford, Versatile methods for the fabrication of polyvinylidene fluoride microstructures, Macro. Rapid. Commun., in review.
[19] M. VanLandingham, Review of instrumented indentation, J. Res. NIST. 108 (2003) 249–265.
[20] Y. Wang, K. Ren, Q.M. Zhang, Direct piezoelectric response of piezopolymer polyvinylidene fluoride under high mechanical strain and stress, Appl. Phys. Lett. 91 (2007) 222905.
[21] Measurement Specialties, Inc., Piezo Film Sensors Technical Manual, 1999.
[22] G. Bogart, D. Carr, J. Rogers, Fabrications of PVDF gratings: final report for LDRD project 79884, Tech. Re SAND2005–6706, Sandia National Laboratories, 2006.
[23] M. Koucky, Piezoelectric polymer microstructures for biomedical applications, Master's thesis, The Ohio State University, Columbus, Ohio, 2009.
[24] A. Dubach, R. Raghavan, J. Löffler, J.J. Michler, U. Ramamurty, Micropillar compression studies on a bulk metallic glass in different structural states, Scr. Mater. 60 (2009) 567–570.
[25] L. Lee, M. Madou, K. Koelling, S. Daunert, S. Lai, C. Koh, Design and fabrication of CD-like microfluidic platforms for diagnostics: Microfluidic functions, Biomed. Microdevices 3 (2001) 245–254.
[26] N. Ferrell, J. Woodard, D. Hansford, Fabrication of micro- and nanoscale polymer structures by soft lithography and spin dewetting, Biomed. Microdevices 28 (2007) 966–971.

Biographies

Jian Xu received BE and ME degrees in Mechanical Engineering from Tsinghua University, China, in 1998 and 2003, respectively. He is currently working toward the PhD degree in Mechanical Engineering at The Ohio State University. His current research is focused on PVDF based acoustic sensors for sound measurements. He has worked on various projects including epidural needle insertion simulator, VISMATLAB, design and analysis of an intelligent paint booth air conditioning control system for Honda Marysville automobile plant, design and development of the first rapid prototyping machine based on the process, Fused Deposition Modeling, in China, etc. He was the recipient of a University Fellowship at Ohio State.

Marcelo Dapino is an Associate Professor of Mechanical Engineering and Director of the Smart Materials and Structures Laboratory. Professor Dapino has made substantial scientific and applied contributions through his work on experimental characterization and thermodynamics-based constitutive modeling of nonlinear active materials. Professor Dapino is a principal investigator on several research programs sponsored by industry and government agencies, including among others DARPA, NSF, DOE, ONR, Dana Tokai Rubber, American Axle & Manufacturing, Edison Welding Institute, Moog, Honda R&D, Boeing, Solidica, and Advanced Numerical Solutions. He serves as a core investigator on an Office of Naval Research Multidisciplinary University Research Initiative (MURI) on iron-based magnetostrictive alloys and a National Science Foundation Industry/University Collaborative Research Center on Smart Vehicle Concepts. As author of over 110 technical publications in journals, edited volumes, and conference proceedings, and recipient of several "Best Paper" awards by the American Society of Mechanical Engineers (ASME) and the International Society for Optical Engineers (SPIE), Professor Dapino is a recognized leader in the field of active material systems. He has served as Chair of the Behavior and Mechanics of Multifunctional and Composite Materials Conference of the SPIE International Symposium on Smart Structures and Materials and is Co-Chair to the ASME Adaptive Structures and Material Systems Technical Committee.

Daniel Gallego received his BS degree in Biomedical Engineering from the Antioquia School of Engineering (EIA), Envigado, Colombia, in 2003. Mr. Gallego worked as a Research Associate at EIA from 2004 to 2005. He is currently working towards the PhD degree in Biomedical Engineering at The Ohio State University, Columbus, OH, USA. His research interests include Biomaterials, BioMEMS and Tissue Engineering.

Derek Hansford is a joint faculty member with Biomedical Engineering and the Biophysics graduate program at OSU. He has more than eleven years of research experience on microelectromechanical systems (MEMS). This experience ranges from characterization of the operational and material characteristics of silicon micromotors and microresonators to the development of complete microfabrication protocols of polymers with specifically designed functional groups. His current research involves the development of generalized microfabrication protocols for polymers as well as advanced applications of polymer, glass, and silicon microdevices for biomedical applications. Dr. Hansford serves as the Chief Scientist of Microfabrication at the Nanotech West Laboratory. In this role, he supervises and performs research on novel processing technologies for biomedical microdevices, including materials thin film research and device design and fabrication research. He also works with other researchers to implement their processes in the lab, assists researchers new to microfabrication in developing microfabrication protocols, and develops new processes based on biocompatible materials.